### Title

Full-field ultrasonic inspection for a composite sandwich plate skin-core debonding detection using laser-based ultrasonics




### ISBN

978-1-5106-0825-2



### Authors

Chong, See Yenn
Victor, Jared J
Todd, Michael D



### Publication Date

2017-04-05

### DOI

10.1117/12.2258574

Peer reviewed

# Full-field ultrasonic inspection for a composite sandwich plate skin-core debonding detection using laser-based ultrasonics

See Yenn Chong*[a], Jared J Victor[b], Michael D Todd[a]
[a]Department of Structural Engineering, University of California, San Diego, 9500 Gilman Dr., La Jolla, CA, USA 92093; [b]R&D Emerging Technologies – Aerostructures, UTC Aerospace Systems, 850 Lagoon Dr., Chula Vista, CA, USA 91910

## ABSTRACT

In this paper, a full-field ultrasonic guided wave method is proposed to inspect a composite sandwich specimen made for an aircraft engine nacelle. The back skin/core interface of the specimen is built with two fabricated disbond defects (diameters of 12.7 mm and 25.4 mm) by removing areas of the adhesive used to bond the back skin to the core. A laser ultrasonic interrogation system (LUIS) incorporated with a disbond detection algorithm is developed. The system consists of a 1-kHz laser ultrasonic scanning system and a single fixed ultrasonic sensor to interrogate ultrasonic guided waves in the sandwich specimen. The interest area of 400 mm × 400 mm is scanned at a 0.5 mm scan interval. The corresponding full-field ultrasonic data is obtained and generated in the three-dimensional (3-D) space-time domain. Then, the 3-D full-field ultrasonic data is Fourier transformed and the ultrasonic frequency spectra are analyzed to determine the dominant frequency that is sensitive to the disbond defects. Continuous wavelet transform (CWT) based on fast Fourier transform (FFT) is implemented as a single-frequency bandpass filter to filter the full-field ultrasonic data in the 3-D space-time domain at the selected dominant frequency. The LUIS has shown the ability to detect the disbond with diameters of 11 mm and 23 mm which match to the pre-determined disbond sizes well. For future research, a robust signal processing algorithm and a model-based matched filter will be investigated to make the detection process autonomous and improve detectability.

**Keywords:** Guided waves, laser ultrasound, honeycomb sandwich, skin-core debonding

## 1. INTRODUCTION

Honeycomb sandwich structures are widely used in the aerospace, marine, automotive and recreational industries because of their superior bending stiffness, low weight, and potential acoustic damping. However, it is important to consider the quality of the skin-core bonding that is highly dependent on the curing method applied as well as the bonding properties between the honeycomb core and face sheet. In many cases, skin-core debonds may also occur due to the adhesive bond degradation in an aging structure caused by thermo-mechanical aging and impact loading [1, 2].

Skin-core debonds can substantially lessen the performance of the sandwich structure and could potentially lead to failure of the bond panel. Damage detection in composite sandwich structures is particularly difficult because the skin-core configuration conceals damage. Therefore, it is vital to accurately identify those hidden defects to prevent failure of such structures. This has led to extensive research in non-destructive evaluation (NDE) techniques for diagnosing sandwich structure damage, especially in aerospace and marine industries. In recent studies, researchers have investigated disbond detection in honeycomb sandwich structures by using guided waves with contact and non-contact ultrasonic transducers [3-8]. In particular, ultrasonic non-destructive evaluation techniques based on guided waves have been highly acknowledged and widely studied for several decades [9-11]. This is primarily due to the fact that plane guided waves have an advantage over conventional through-the-thickness ultrasound due to their greater propagation distances and sensitivity to small defects in structures.

Much research has also utilized Lamb wave propagation, using the leaky Lamb waves (LLW) method for sandwich structures [2, 12]. Bourasseau et al. [12] proposed a contact method to detect the low velocity impact damage in a honeycomb sandwich plate by using the Lamb waves generated by wedge transducers. The study used the LLW phenomenon to detect damage and the S0 mode at relatively high frequencies showed the ability to detect the

* Corresponding author. Email: s3chong@eng.ucsd.edu; phone 1 858 534-5993

delamination between the face sheet and the core. Diamanti et al. [14] applied the A0 mode of Lamb waves at low frequencies (15 and 20 kHz) by using piezoelectric transmitters/receivers to determine the location and extent of face sheet-core debonding and crushed core in honeycomb sandwich beams. The technique is only suitable for global detection because it could not accurately characterize and size damage, since the technique is poor and closely spaced damage areas cannot be separately identified.

For non-contact ultrasonic transducers options, laser ultrasonic techniques (LUTs) have been intensively developed to target large scale inspection, especially in the aeronautics industry. LUTs can be incorporated in laser ultrasonic visualization techniques for quantitative NDE applications [1]. The measurement result can be demonstrated in the 3-D space-time volume and intuitively interpreted without prior in-depth knowledge of ultrasound [15, 16].

In general, laser Doppler vibrometers (LDV) and/or Q-switched pulsed lasers (QL) are employed in LUT where the LDV acted as a sensor and QL acted as an actuator. In Ref. [8], a Piezoelectric-LDV configuration (piezoelectric used as an actuator) was used to obtain guided wave fields and the wavenumber of the full-field was analyzed. The study demonstrated that the incident guided waves excited at 15 kHz have a strong wave interaction in the disbond area, simulated by an area that was made with no honeycomb core (58 mm × 58 mm). Han et al. [6] used a Piezoelectric-LDV configuration to inspect a honeycomb sandwich panel based on imaging of local resonance behavior. The entire honeycomb panel was excited continuously with a single, steady tone at the resonance frequency (32 kHz) of the single pristine and out-of-spec cell using a fixed position transducer. The results show the high-amplitude response in pristine cells and the lower-amplitude response in out-of-spec cells. Additionally, a near-zero response near the cell boundaries and the non-zero response in the damaged cell walls was observed. Q-switched lasers have been widely used in non-destructive testing and evaluation applications. Hence, QL serve as an alternative approach by replacing a conventional contact piezoelectric transducer to generate ultrasound in mechanical structures based on the thermoelastic principle [17]. Chia et al. [18] used a QL-Piezoelectric configuration (Piezoelectric used as an sensor) for impact damage detection in a radome made of glass/epoxy face sheets and a honeycomb core based on the ultrasonic frequency tomography and wavelet-transformed ultrasonic imaging methods in the full-field ultrasonic data. On the other hand, Choi et al. [5] proposed dual-energy wave subtraction imaging for barely visible impact damage (BVID) detection on a sandwich panel with Nomex® honeycomb core in a QL-Piezoelectric configuration. The sandwich panel was inspected at two different laser excitation energy levels and BVID was identified based on the difference of ultrasonic amplitude level.

In this paper, a laser ultrasonic interrogation system based on the QL-Piezoelectric configuration is proposed to investigate the feasibility of disbond detection on a composite sandwich panel made for an aircraft engine nacelle. The front face sheet is perforated and the predetermined disbond defects are induced in between the solid back face sheet and the honeycomb core. In order to investigate the feasibility of using laser-generated ultrasound for disbond detection in sandwich panels, CWT based on FFT is proposed to design a narrow bandpass filter to filter the ultrasound data. Then, the response of the ultrasound with narrowband frequency to the debonding defect is investigated and analyzed.

## 2. EXPERIMENTAL SETUP

### 2.1 Laser Ultrasonic Interrogation System Configuration

Figure 1(a) shows a schematic diagram of a laser ultrasonic interrogation system, which consists of a laser scanning system incorporated with a signal conditioning device, a data acquisition (DAQ) module, a contact sensor, and a computer used for signal processing and operation control. As shown in Fig. 1(b), the laser scanning system has a two-dimensional (2-D) laser scanner and a diode-pumped solid-state Q-switched Nd:YAG laser. The Q-switched laser is composed of a laser controller and a laser head with output beam of 527 nm wavelength and pulse repetition rates (PRR) from single-shot to 1 kHz. The Q-switched laser can produce average pulse energy of up to 1 mJ at the PRR of 1 kHz. The 2-D laser scanner is used to synchronize the 2-axis galvanometer scanner (Fig. 1(a)) with the Q-switched laser to maneuver the laser impinging point rapidly on a target at a PRR to perform a raster scanning process. In the scanning process, a laser pulse is impinged at a scan point and the corresponding ultrasound is generated at the local point based on the thermoelastic principle. The generated ultrasound is then signal-conditioned through a contact sensor and digitized in the DAQ module as shown in Fig. 1(a). In the DAQ module, the generated ultrasound is digitized synchronously with the PRR of the laser scanning system by receiving a triggering signal from the laser controller after the laser pulse is emitted. In the digitizing process, the ultrasound is sampled for $N$ number of data points at sampling time interval $T_S$ and stored in a computer. The digitizing process is repeated as the scanning process is performed. Once

the scanning process is completed, the ultrasound in 2-D space with $X$ and $Y$ grid of points on the target are generated and all generated ultrasonics are generated in the form of a three-dimensional (3-D) $X$ by $Y$ by $N$ matrix, indexed by spatial-$x$-direction, spatial-$y$-direction, and $n$ time sample, respectively, along each dimension. Lastly, the 3-D ultrasonic data, denoted as $u(x, y, t)$, is further processed and analyzed in the computer.

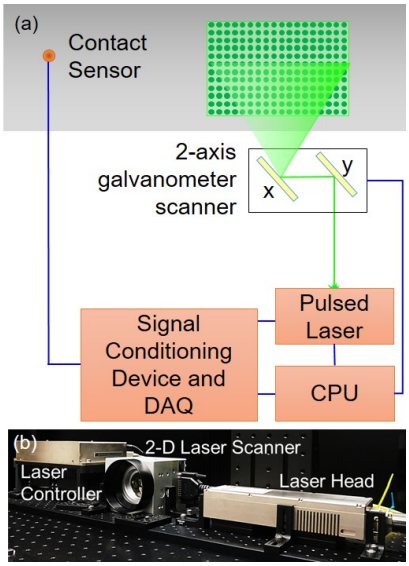


Figure 1. (a) Laser ultrasonic interrogation system configuration and (b) Q-switched pulsed laser parts.

In this paper, the PRR of the laser scanning system was set at 1 kHz with the pulsed energy of 1 mJ (fluence of 23 mJ/cm$^2$). A honeycomb sandwich panel was set up at a stand-of-distance of 1770 mm from the 2-D laser scanner. In Fig. 2(a), an area of 400 mm × 400 mm on the front face sheet of the panel was scanned with a scan interval of 0.5 mm and a PZT sensor (APC-851-WFB) bonded at the center of the front face sheet. An in-line bandpass filter was used in this research to filter ultrasonic signals at the frequency range of 30-200 kHz since the low frequency of guided ultrasonic wave are widely used for skin-core disbond detection [3, 6, 8, 19]. Next, the ultrasonic signal is sampled by the DAQ module with a sampling time of $T_S$ = 0.4 μs and $N$ = 1000 total sample points. Since honeycomb sandwich structures have inherent heavy damping, scanning was repeated 15 times, and the generated ultrasonic signals were then averaged to obtain an improved signal-to-noise (SNR) of the generated ultrasonic signals [20]. Lastly, the 3-D $X$ by $Y$ by $N$ matrix ultrasonic wavefield was obtained and stored in a computer for further analysis.

### 2.2 Honeycomb Sandwich Panel Configuration

Figure 2(a) shows a schematic diagram of the honeycomb sandwich panel configuration used in this research. The panel was fabricated to the dimensions of 457.2 mm × 457.2 mm × 11 mm (height × width × thickness) and was composed of two plain weave CFRP face sheets and an aluminum honeycomb core. The front and back face sheets have ply orientations of [0/±45/90] and [$0_3$] and total thicknesses of 0.8 mm and 1.2 mm, respectively. The front face sheet was perforated with diameters around 1.2 mm [Fig. 2(a)], while the back face sheet had five metallic attachment hardware bolts bonded to it [Fig. 2(b)]. To investigate the feasibility of disbond detection using LUIS, two predetermined disbonds were introduced between the back face sheet and the aluminum honeycomb core. The adhesive layer used to bond both surfaces had cut-through circles of different sizes at two different predefined locations. The diameters of the circle were set to 25.4 mm (1.0”) and 12.7 mm (0.5”) and the respective predefined locations (denoted as $A$ and $B$) were located at the distances of 63.5 mm and 127.0 mm away from the center of the panel as shown in Fig. 2(a).

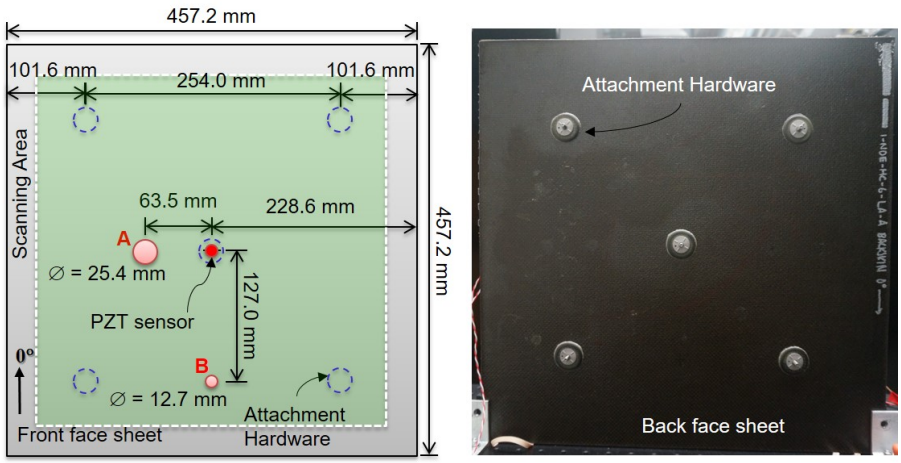


Figure 2. CFRP/Al honeycomb sandwich panel: (a) disbond defects (denoted as *A* and *B*) and dimension configurations and (b) attachment hardware configuration at back face sheet.

## 3. DISBOND DETECTION PROCESS

In previous studies, leaky Lamb waves were used in detecting composite or composite honeycomb sandwich disbonds, but the resulting wave is very complex due to interaction between multi-frequencies. Besides that, there is no precise information regarding the dominant scattering frequency of the disbond defect in the present study. So, in order to improve the signal to noise ratio of the disbond detection, the local dominant frequencies of the predetermined disbond defects (Fig. 2(a)) are determined first in this paper. Then, a narrow bandpass filter based on continuous wavelet transform is used to filter to obtain the dominant frequency for all scan-points $(x, y)$. The filtered ultrasound is denoted as $\tilde{u}_{\langle f_{\mathrm{BW}} \rangle}(x,y,t)$ and $f_{\mathrm{BW}}$ is the narrow passband frequency. Lastly, $\tilde{u}_{\langle f_{\mathrm{BW}} \rangle}(x,y,t)$ is analyzed to detect the disbond.

### 3.1 Frequency Spectral Analysis

To obtain accurate dominant frequencies, all ultrasonic signals regardless of their attenuation should be considered. Hence, ultrasounds generated along the circumference of a circle with a fixed radius $R$ from a source point, are considered to be the dominant frequencies. In the scanning processing (Fig. 1(a)), ultrasounds are generated at the scan points based on Cartesian coordinate scheme. So, ultrasounds of $u(r,\theta,t)$ along the radius of $r$ in polar coordinate are obtained by converting the $u(x,y,t)$ with the following expressions:

$$r = \sqrt{x^2 + y^2} \tag{1}$$

and

$$\theta = \tan^{-1}\left(\frac{y}{x}\right), \tag{2}$$

where $x$ and $y$ are the indices of the 2-D spatial domain and $\theta$ is the angles of the circumference from 0° to 359°. Since the ultrasonic wavefield propagation imaging is generated based on the reciprocity of ultrasonic propagation [16], the sensor located at the sandwich panel (Fig. 2(a)) was set as the central point of the polar plot. With the Eqns. (1) and (2), ultrasounds of $u(R,\theta,t)$ are determined. In this paper, a fixed radius $R$ of 63.5 mm was set to $r$ where the disbond was located as shown in Fig. 2(a) and this is to ensure the possible dominant frequency of the disbond is included in the analysis later. The $\theta = 0°$ was set at the coordinate of $(63.5, 0)$. After that, the ultrasounds of $u(R,\theta,t)$ are transformed using Fourier transform (FT) and the frequency spectra of the ultrasounds are obtained and denoted as $u(R,\theta,f)$. Then,

the spectra are represented in a normalized power spectral density (PSD) plot for the dominant frequency estimation. For disbond *B*, the same process discussed above was repeated except *R* was set to 127.0 mm.

### 3.2 Narrow Bandpass Filter based on Continuous Wavelet Transform

In this section, a narrow bandpass digital filter is used to filter the ultrasound of $u(x, y, t)$ for all scan points and the narrow passband frequency is set based on the dominant frequency determined in the previous section.

A digital filter is usually designed based on either the finite impulse response (FIR) method or the infinite impulse response (IIR) method. To design a narrow bandpass filter, both methods must configure with a longer impulse response and higher filter order to obtain a steeper passband transition. In result, it increases phase shift distortion in the filtered signal [13, 21]. Due to this constraint, continuous wavelet transform (CWT) filtering methods [22-24] are used for digital filter applications as an alternative method. In this research, CWT based on FFT is adopted to design a narrow bandpass filter to filter an ultrasonic signal with the narrow passband frequency range.

In principle, the CWT computes the inner product of a signal $s(t)$ with translated and dilated version of an analyzing wavelet, $\psi$ (also named as mother wavelet). The definition of the CWT is

$$C(a,b) = \frac{1}{\sqrt{a}} \int_{-\infty}^{+\infty} s(t) \psi^* \left( \frac{t-b}{a} \right) dt \ , \tag{3}$$

where $\psi^*(\bullet)$ is the complex conjugate of the mother wavelet function and *b* and *a* are the translation and scale parameters, respectively. However, the CWT expressed in Eqn. (3) is time-consuming for computational calculations. In recent years, the fast Fourier transform algorithm has been used to calculate the CWT to accelerate the computation time and Eqn. (3) can be interpreted as a frequency-based filtering of the signal by rewriting the CWT as an inverse FT in the following form [23, 25, 26]

$$C(a,b) = \frac{1}{2\pi} \int_{-\infty}^{+\infty} \hat{s}(\omega) \hat{\psi}^*(\omega) \, d\omega \ , \tag{4}$$

where

$$\hat{\psi}^*(\omega) = \sqrt{a} \hat{\psi}^*(a\omega) e^{i\omega b} \tag{5}$$

and

$$\hat{s}(\omega) = \int_{-\infty}^{+\infty} s(t) e^{-i\omega t} dt \tag{6}$$

denotes the FT of the mother wavelet at scale *a* and translation *b*, and the FT of the signal $s(t)$, respectively. In this paper, $s(t)$ is the ultrasonic signal $u(x, y, t)$ and Bump wavelet was considered. Bump wavelet was considered because it has a relatively smaller frequency support that lead to a better frequency localization of the ridge [27].

As in implementation, the scales *a* must be determined first, which is relative to the passband frequency with low-cutoff frequency and high-cutoff frequency. The corresponding wavelet coefficients (Eqn. (4)) are then obtained by substituting the scale *a* into the *cwtft* function in MATLAB 2015b [23]. Lastly, the filtered ultrasound $\tilde{u}_{\langle f_{\mathrm{BW}} \rangle}(x, y, t)$ can be obtained by inversely transforming the wavelet coefficients using the *icwtft* function in MATLAB 2015b [23]. For an example, as shown in Fig. 3, an ultrasound generated with the frequency range of 30-200 kHz in the proposed sandwich panel was bandpass filtered at the low-cutoff and high-cutoff frequencies of 170 and 180 kHz respectively. Figure 3(a) shows the time-history and the comparison between unfiltered and filtered ultrasounds. The filtered ultrasound showed that the dominant wave packet has the same phase with the unfiltered ultrasound in between 20 μs to 100 μs. Figure 3(b) shows that the frequency response of the ultrasounds in the normalized power spectral density plot and the frequency spectra of the filtered ultrasound match well with the unfiltered ultrasound. For that, a narrow bandpass filter using CWT based on FFT is suitable for a narrow bandpass filtering application with no delay time in the filtered signal as compared to the

FIR/IIR method [13, 21]. After the filtering process, the filtered full-field ultrasonic response is analyzed frame by frame to analyze the disbond detectability. Afterwards, the narrowband ultrasound is obtained and the response wave in the space-time domain to the disbond defect is further analyzed.

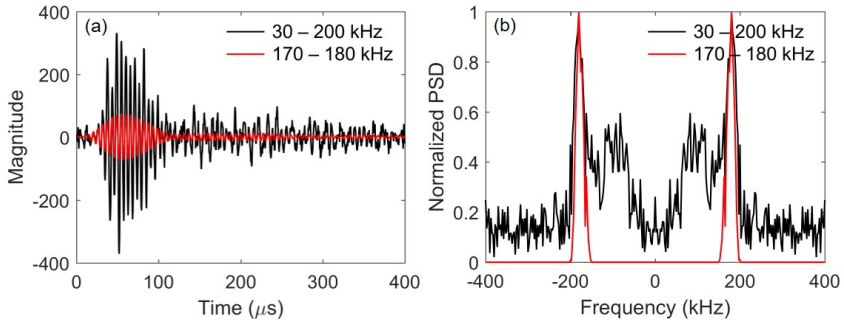


Figure 3. Ultrasonic signals with broad and narrow passband frequencies comparison in (a) time-history and (b) frequency-history.

## 4. RESULTS AND DISCUSSIONS

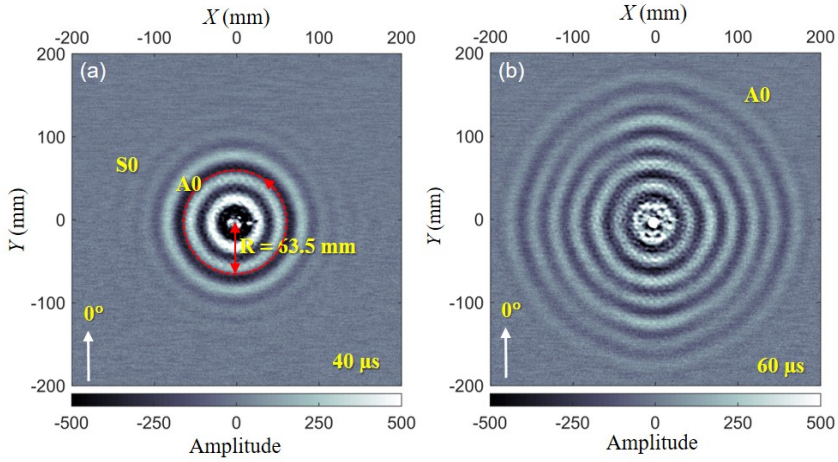


Figure 4. Ultrasonic wavefield imaging at (a) 40μs and (b) 60μs in the frequency range of 30-200 kHz.

Figure 4 shows the ultrasonic wavefield imaging for the composite sandwich panel plotted in a Cartesian coordinate system with the *x*-axis and y-axis ranging from –200 mm to 200 mm. The sensor was coordinated at $(0,0)$ and the two predetermined disbonds were located at $A(-63.5,0)$ and $B(0,-127.0)$ respectively. The ultrasonic waves propagating out from the sensor $(0,0)$ were created based on the reciprocity principle of ultrasonic propagation [16].

The ultrasonic wavefield imaging at 40 μs (Fig. 4(a)) showed the wavefronts of the S0 and A0 modes emerged as the wavefront propagated out from the sensor. The wavefront of the S0 mode exhibited significantly weak amplitude. In contrast, the wavefront of the A0 mode exhibited strong amplitude dominance. As the A0 mode propagated at 60 μs, the wave-honeycomb core interaction can be seen as illustrated in Fig. 4(b) and this is due to the energy leaked into the honeycomb core from the upper skin panel [19, 28, 29]. The guided wave energy in the top skin not only leaked into the honeycomb core it also transmitted to the bottom skin and induced guided wave motions in the bottom skin. However, the wavefield imaging showed no anomaly wave after the wavefronts of A0 mode flowed through the disbond area $A\,(-63.5,0)$. In conclusion, the disbond at the back face sheet could not be detected based on the A0 mode with the frequency band of 30-200 kHz.

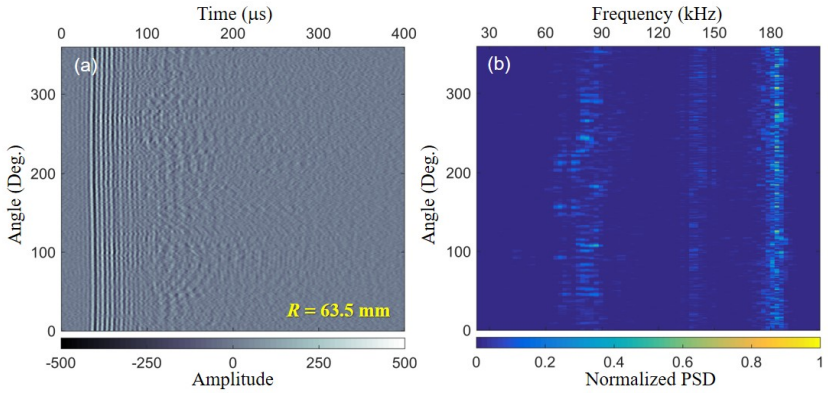


Figure 5. Ultrasonic signals at the radius of 63.5 mm (a) in angle-time and (b) angle-frequency domains.

In Fig. 5(a), the ultrasounds at the circumference with $R$ = 63.5 mm were obtained (Eqns. (1) and (2)) and plotted in the angle-time domain. After the one-dimensional (1-D) Fourier transform to $u(R,\theta,t)$, the corresponding frequency spectra were plotted in the angle-frequency domain with the normalized PSD [Fig. 5(b)]. The frequency spectra showed high power in the frequency ranges of 60-90 kHz and 170-190 kHz. The frequency of 140 kHz was neglected in this paper since the power level was significantly lower than the other two frequency ranges. The power of the frequency spectra (60-90 kHz and 170-190 kHz) in the angle-frequency domain was well distributed and consistent at all angles. However, in the 60-90 kHz range, the wave energy showed a change around the angles from 150° to 250° where the disbond was located. This is why the narrow frequency band between $f_{BW1}$ = 60-70 kHz, $f_{BW2}$ = 70-80 kHz, and $f_{BW3}$ = 80-90 kHz was selected as the passband in the narrow bandpass filter. The filter with the passbands of $f_{BW4}$ = 170-180 and $f_{BW5}$ = 180-190 kHz was considered as well to investigate the response of the ultrasound at the high frequency range. Next, all wavefield images are plotted in the $x$-axis range of –200 mm to 0 mm and $y$-axis range of –100 mm to 100 mm for better visibility of images results.

With the dominant frequencies determined in the previous step, $u(x,y,t)$ was filtered using the narrow passband frequency of the proposed filter. Figure 6 shows the freeze-frames of the ultrasonic wavefield imaging with the passbands of $f_{BW1}$, $f_{BW2}$, and $f_{BW3}$ based on Eqn. (4). In Fig. 6(a), the wavefield imaging of $\tilde{u}_{\langle f_{BW1}\rangle}$ at 148.8 μs showed the detection of the defect. For better view, Fig. 6(a) was further zoomed in and shown in Fig. 6(b) where the disbond shape was identifiable with the estimated diameter of about 23 mm at the location $(-63.5, 0)$. The estimation showed good agreement with the predefined defect size and location. As for $\tilde{u}_{\langle f_{BW2}\rangle}$ at 108.8 μs in Fig. 6(c), the diameter of the debond was estimated to be less than 15 mm, which is less accurate than $\tilde{u}_{\langle f_{BW1}\rangle}$ and the disbond was barely detected in $\tilde{u}_{\langle f_{BW3}\rangle}$ at 104.4 μs [Fig. 6(d)]. Since the adhesive layer with a cut-through circle was used to form an artificial disbond between the back face sheet and the honeycomb core it might possible that the two surfaces were not debonded completely during the curing process. Therefore, the wave energies of the $\tilde{u}_{\langle f_{BW2}\rangle}$ and $\tilde{u}_{\langle f_{BW3}\rangle}$ were leaked into the honeycomb core, reached the back face sheet, and formed the wave-honeycomb interaction as shown in Figs. 6(c) and (d) respectively. In contrast, the wave energy of $\tilde{u}_{\langle f_{BW1}\rangle}$ leaked into the honeycomb core but it was not able to reach the back face sheet. Hence, the wave was only resonant at the local honeycomb core and formed a donut-shape, which is indicated as a disbond in Figs. 6(a) and (b).

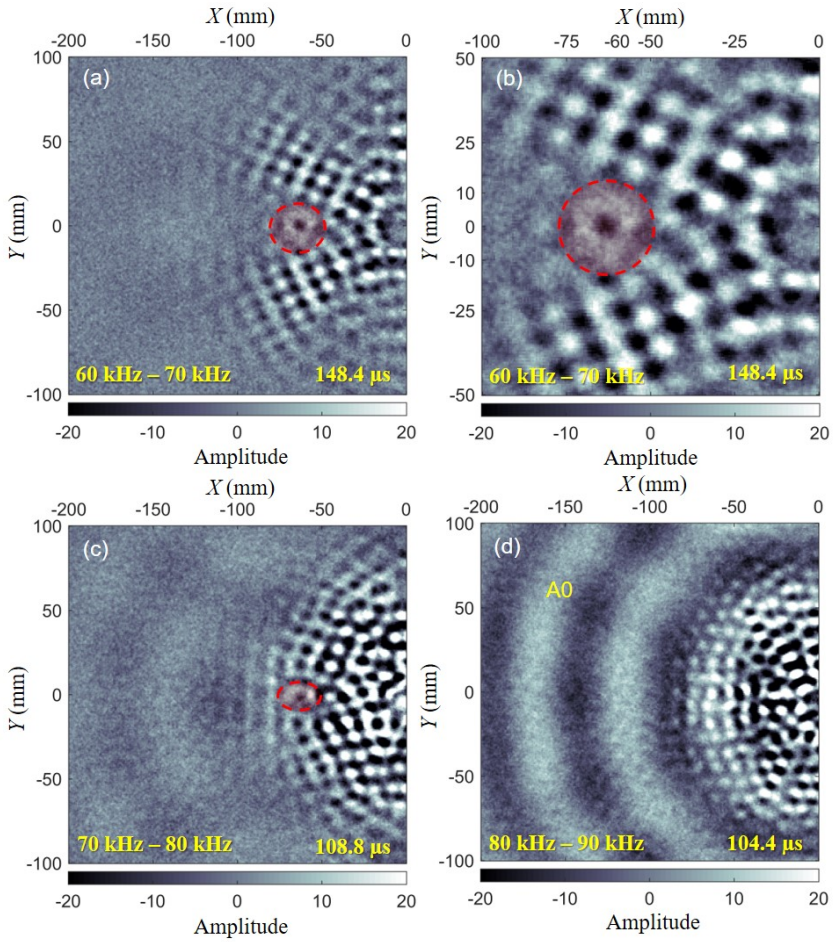


Figure 6. Ultrasonic wavefield imaging with the narrowband frequency of (a)(b) 60-70 kHz, (c) 70-80 kHz, and (d) 80-90 kHz.

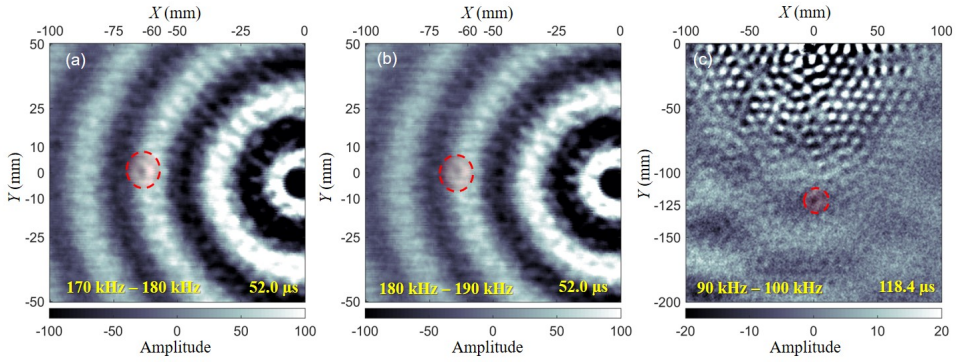


Figure 7. Ultrasonic wavefield imaging with the narrowband frequency of (a) 170-180 kHz, (b) 180-190 kHz and (c) 90-100 kHz.

Figures 7(a) and (b) show the freeze-frames of the ultrasonic wavefield imaging with the passbands of $f_{BW4}$ and $f_{BW5}$. The ultrasonic wavefield for both passbands showed the detection of the disbond at 52.2 µs. A disbond diameter of about 16

mm was estimated and is less accurate as compared to the case in Fig. 6(a). The disbond visibility was also weak as compared to the previous two cases illustrated in Figs. 6(b) and (c). Disbond *B* has the same dominant frequencies as shown in Fig. 5(b). Figure 7(c) shows that the disbond was barely detected only with the narrowband frequency of 90-100 kHz. The diameter was moderately estimated around 11 mm. The low visibility and accuracy might due to the size of the disbond was similar to the size of the honeycomb cells.

## 5. SUMMARY

A laser ultrasonic interrogation system was developed to inspect a composite sandwich panel of an aircraft engine acoustic liner with two programmed disbond defects (diameters of 12.7 mm and 25.4 mm). The 3-D ultrasound in space-time domain at the range of 30-200 kHz showed no evidence on the programmed disbands, but the data were used to determine dominant frequencies of the disbond defects, which was used to filter the 3-D ultrasound in space-time domain data. The 3-D filtered ultrasound at the range of 60-70 kHz passband frequency was shown to detect the disbond defect with the diameter deviation of less than 8% from the pre-defined diameter (25.4 mm). But, as the passband frequency increased, the diameter deviation was increased to 37% in the passband frequencies of 170-180 kHz and 180-190 kHz. The high deviation was suspected due to the disbond area was not debonded completely. As for the disbond *B*, only passband frequency of 90-100 kHz has shown the detection of the disbond with the estimated diameter of 11 mm. However, the visibility of the disbond in the images was low and difficult to localize without prior knowledge of the disbond location. For future research, a robust signal processing algorithm and a model-based matched filter will be investigated to make the detection process autonomous and to improve detectability. The filtered ultrasound using CWT shows no time-delay and the frequency response of the filtered ultrasound matches well to the preset passband frequency of the filter.

## ACKNOWLEDGEMENTS

The authors acknowledge the support of UTC Aerospace Systems for sponsoring this research.

## REFERENCES

[1] Achenbach, J. D., “Quantitative nondestructive evaluation,” International Journal of Solids and Structures 37(12), 13-27 (2000).

[2] Takeda, N., Minakuchi, S., and Okabe, Y., “Smart composite sandwich structures for future aerospace application-Damage detection and suppression-: A review,” Journal of Solid Mechanics and Materials Engineering 1, 3-17 (2007).

[3] Chakraborty, N., Rathod, V., Mahapatra, D. R., and Gopalakrishnan, S., “Guided wave based detection of damage in honeycomb core sandwich structures,” NDT & E International 49, 27-33 (2012).

[4] Chapuis, B., Kulakovskyi, A., Bedreddine, N.-R., and Dalmeida, O., “Development of an SHM system of sandwich composite panels using guided elastic waves,” 8th European Workshop On Structural Health Monitoring (2016).

[5] Choi, Y. and Lee, J.-R., “Dual-energy wave subtraction imaging for damage detection in ultrasonic propagation imaging system,” in 2016 IEEE Aerospace Conference: IEEE, 1-6 (2016).

[6] Han, S., Lee, J.-R., and Flynn, E.B., “Remote imaging of local resonance for inspection of honeycomb sandwich composite panels,” in SENSORS, 2015 IEEE, 1-4 (2015).

[7] Song, F., Huang, G., and Hu, G., “Online guided wave-based debonding detection in honeycomb sandwich structures,” Aiaa Journal 50, 284-293 (2012).

[8] Tian, Z., Yu, L., Huang, G., van Tooren, M., and Mitchell, W., “Wavenumber study of guided waves in aluminum honeycomb sandwich structures,” SPIE Smart Structures and Materials + Nondestructive Evaluation and Health Monitoring: International Society for Optics and Photonics, 943807-943807-8 (2015).

[9] Giurgiutiu, V. and Cuc, A., “Embedded non-destructive evaluation for structural health monitoring, damage detection, and failure prevention,” Shock and Vibration Digest 37, 83 (2005).

[10] Raghavan, A. and Cesnik, C. E., “Review of guided-wave structural health monitoring,” Shock and Vibration Digest 39, 91-116 (2007).
[11] Rose, J. L., [Ultrasonic waves in solid media], Cambridge university press (2004).
[12] Bourasseau, N., Moulin, E., Delebarre, C., and Bonniau, P., “Radome health monitoring with Lamb waves: experimental approach,” NDT & E International 33, 393-400 (2000).
[13] Allen, D. P. and MacKinnon, C. D., “Time–frequency analysis of movement-related spectral power in EEG during repetitive movements: a comparison of methods,” Journal of neuroscience methods186, 107-115 (2010).
[14] Diamanti, K., Soutis, C., Hodgkinson, J. M., “Lamb waves for the non-destructive inspection of monolithic and sandwich composite beams,” Composites Part A: Applied Science and Manufacturing 36, 189-195 (2005).
[15] Staszewski, W., Lee, B., Mallet, L., and Scarpa, F., “Structural health monitoring using scanning laser vibrometry: I. Lamb wave sensing,” Smart Materials and Structures13, 251 (2004).
[16] Takatsubo, J., Wang, B., Tsuda, H., and Toyama, N., “Generation Laser Scanning Method for the Visualization of Ultrasounds Propagating on a 3-D Object with an Arbitrary Shape,” Journal of Solid Mechanics and Materials Engineering 1, 1405-1411 (2007).
[17] Scruby, C. B. and Drain, L. E., [Laser ultrasonics techniques and applications], CRC Press (1990).
[18] Chia, C. C., Lee, J.-R., and Park, C. Y., “Radome health management based on synthesized impact detection, laser ultrasonic spectral imaging, and wavelet-transformed ultrasonic propagation imaging methods,” Composites Part B: Engineering 43, 2898-2906 (2012).
[19] Song, F., Huang, G., and Hudson, K., “Guided wave propagation in honeycomb sandwich structures using a piezoelectric actuator/sensor system,” Smart Materials and Structures 18, 125007 (2009).
[20] Lee, J.-R., Chong, S. Y., Sunuwar, N., and Park, C. Y., “Repeat scanning technology for laser ultrasonic propagation imaging,” Measurement Science and Technology 24, 085201 (2013).
[21] Klepka, A. and Uhl, T., “Identification of modal parameters of non-stationary systems with the use of wavelet based adaptive filtering,” Mechanical Systems and Signal Processing 47, 21-34 (2014).
[22] Ma, J. C., Luo, L., and Wu, Q. B., “A filter design method based on combination wavelets,” Mechanical Systems and Signal Processing 11, 767-72 (1997).
[23] Misiti, M., Misiti, Y., Oppenheim, G., and Poggi, J.-M., “Matlab Wavelet Toolbox User\'s Guide. Version 4.15,” (2015).
[24] Park, H. W., Sohn, H., Law, K. H., and Farrar, C. R., “Time reversal active sensing for health monitoring of a composite plate,” Journal of Sound and Vibration 302, 50-66 (2007).
[25] Komorowski, D. and Pietraszek, S., “The Use of Continuous Wavelet Transform Based on the Fast Fourier Transform in the Analysis of Multi-channel Electrogastrography Recordings,” Journal of medical systems 40, 1-15 (2016).
[26] Li, L.-c., “A new method of wavelet transform based on FFT for signal processing,” 2010 Second WRI Global Congress on Intelligent Systems: IEEE 3, 203-206 (2010).
[27] Sharma, T. and Sharma, K. K., “Power line interference removal from ECG signals using wavelet transform based component-retrieval,” Advances in Computing, Communications and Informatics (ICACCI), 2016 International Conference on: IEEE, 95-101 (2016).
[28] Mustapha, S. and Ye, L., “Leaky and non-leaky behaviours of guided waves in CF/EP sandwich structures,” Wave Motion 51, 905-918 (2014).
[29] Tian, Z., Huang, G., and Yu, L., “Study of Guided Wave Propagation in Honeycomb Sandwich Structures,” ASME 2014 Conference on Smart Materials, Adaptive Structures and Intelligent Systems: American Society of Mechanical Engineers V001T05A9-VT05A9 (2014).